Petroleum Science 20 (2023) 1903–1908

Contents lists available at ScienceDirect

Petroleum Science

journal homepage: www.keaipublishing.com/en/journals/petroleum-science

Short Communication

Hydrothermally stable mesoporous aluminosilicates as superior FCC catalyst: From laboratory to refinery

Hong-Tao Liu [a], Jiu-Jiang Wang [b], Fang-Ming Xie [b], Yun-Chuang Li [a], Hai-Yan Li [b], Hai-Yan Liu [c], Yuan-Yuan Yue [d], Xiao-Tong Mi [a], Xiong-Hou Gao [b], Hong-Hai Liu [b, *]

[a] State Key Laboratory of Chemical Resource Engineering, Beijing University of Chemical Technology, Beijing, 100029, China
[b] Petrochemical Research Institute, Petrochina Company Limited, Beijing, 100195, China
[c] State Key Laboratory of Heavy Oil Processing, China University of Petroleum (Beijing), Beijing, 102249, China
[d] National Engineering Research Center of Chemical Fertilizer Catalyst, College of Chemical Engineering, Fuzhou University, Fuzhou, Fujian, 350002, China

ARTICLE INFO

Article history:
Received 12 July 2022
Received in revised form
24 October 2022
Accepted 30 November 2022
Available online 2 December 2022

Edited by Jia-Jia Fei

Keywords:
Mesoporous aluminosilicates
Heavy oil
Fluid catalytic cracking
Industrial application

ABSTRACT

Well-ordered aluminosilicates (MAs) were prepared by *in-situ* assembly of pre-crystallized units of zeolite Y precursors at a commercial scale, and applied in an industrial fluid catalytic cracking unit for the first time. Compared with incumbent equilibrium catalyst, the surface area of trial equilibrium catalysts (30% inventory ratio) increased from 110 $m^2 g^{-1}$ to 120 $m^2 g^{-1}$. Moreover, a significant increase of the mesoporous surface area of trial equilibrium catalysts (30% inventory ratio) from 33 $m^2 g^{-1}$ to 40 $m^2 g^{-1}$ (22% increase). Furthermore, the equilibrium catalyst that contain 80% LPC-65 yields significantly lower heavy oil (0.23%) and higher total liquids (0.53%) compared with LDO-70. The industrial results demonstrated excellent hydrothermal stability and superior catalytic cracking properties, showing the promising future in the industrial units.

1. Introduction

Much attention was paid to the fluid catalytic cracking (FCC) of heavy oil due to its greatly enhanced processing difficulty because of the large molecules (Fu et al., 2006; Puente et al., 2007; Talmadge et al., 2014; Corma et al., 2017). It was well known that FCC of large molecules of heavy oil would be carried out in a successive way: (1) the large heavy oil molecules are precracked firstly in the macropores of the matrix, such as kaolin; (2) the products obtained in step (1) cracked further in the mesopores; (3) the intermediate products of step (2) cracked more selectively to valuable products, such as gasoline, diesel, and other chemical products (Ji et al., 2018). In addition to this, the improvement of FCC catalysts in the face of new challenges (such as new feeds and less polluting products) would be extremely urgent (Valle et al., 2019; Palos et al., 2021). Therefore, it is of vital importance to implant mesoporosity into FCC catalysts of heavy oil.

To date, many approaches to introducing mesoporosity into FCC catalysts have been developed. A typical way is the so-called "top-to-down" method, which involves the removal of Al or Si species of zeolites (Verboekend et al., 2013; Jia et al., 2019). Unfortunately, this process suffers from zeolitic loss due to the destructive route. Another procedure "down-to-up" is a convenient approach to generating mesoporosity directly (Saxena et al., 2014; Kerstens et al., 2020). However, the low hydrothermal stability and high synthesis cost of the obtained materials still hinder its industrial application in severe conditions of FCC. Therefore, how to obtain hydrothermally stable MAs synthesized with low synthesis cost is still a great challenge in both FCC process and materials science.

Our group (Liu et al., 2013a; Cao et al., 2014; Jin et al., 2014; Mi et al., 2018a; Chen et al., 2021; Li et al., 2022) has obtained MAs with excellent hydrothermal stability by a novel strategy that introduces zeolite Y precursors (the primary and secondary structural unit of zeolite Y) into the walls of mesoporosity. Just in this idea, our group obtained MAs with hydrothermal stability comparable to that of USY (Liu et al., 2014a, 2021; Mi et al., 2017a, 2017b, 2018b). For example, the BET surface area of MAs decreased from 595.4 $m^2 g^{-1}$ to 153.9 $m^2 g^{-1}$ after a severe hydrothermal treatment in 100% water vapor at 800 °C for 12 h. Moreover, the materials showed excellent catalytic properties when it was employed in

* Corresponding author.
E-mail address: liuhonghai@petrochina.com.cn (H.-H. Liu).

https://doi.org/10.1016/j.petsci.2022.11.028

heavy oil FCC in the MAT unit (Liu et al., 2013b, 2014b, 2014c; Deng et al., 2022). Although the significant progress in synthesis and application of hydrothermally stable MAs, the commercial manufacturing of materials, preparation of industrial catalysts, and industrial application in pilot FCC unit are still a great challenge for the material scientists.

Herein, we report the most recent progress in commercial manufacturing and catalytic cracking performance in the FCC unit of 1.2-million tons in a refinery. To the best of our knowledge, the research progress represents the most advanced stage of commercial manufacturing and industrial application in FCC of MAs.

2. Experimental section

2.1. Chemical materials

Industrial reagent of Pluronic P123 triblock copolymer ($EO_{20}PO_{70}EO_{20}$) was obtained from Henan Ruiyi Chemical Company. Water glass (containing 27.78 wt% SiO_2 and 8.98 wt% Na_2O) was purchased from Tangshan Shihe Sodium Silicate Company.

2.2. Synthesis of zeolite Y precursors

The mixtures of Na_2SiO_3, $Al_2(SO_4)_3 \cdot 18H_2O$, and NaOH solution with a molar ratio of $Al_2O_3/SiO_2/Na_2O/H_2O$ = 1/16–19/15–20/300–320 were prepared. After rapidly stirring for 30–80 min, the prepared mixtures undergo an ageing with stirring at 80–100 °C for 4–20 h. The obtained sticky solution was denoted as "zeolite Y precursors".

2.3. Industrial synthesis of MAs

(1) P123 and water were added to the reactor. Zeolite Y precursors and H_2SO_4 (6 M) were slowly added to the above reactor to keep the pH of the system at about 1.0–3.0. The obtained solution was stirred at 30–60 °C for 10–40 h.
(2) The liquid product of step (1) were transferred into crystallization autoclaves of 10 m^3 for crystallization under 100–140 °C for 24 h. The as-synthesized products were processed by the subsequent filtering, washing, and drying at 120 °C for 2 h. Then, the resultant solid was calcined at 550 °C for 6 h in order to remove the organic template, the obtained product was denoted as "IS"
(3) IS was hydrothermally aged under a severe condition (800 °C, and 100% water vapor) for 4 h and the product was named as "HIS".

2.4. Characterization

Diffractometer Rigaku D/Max 2500VB2+/PC equipped with Cu Kα radiation was used for the study of X-ray diffraction (XRD) patterns for the obtained samples. JEM 100CX instrument with 200 kV acceleration voltage was used to study the TEM images. A Micromeritics ASAP 2405N system was used to investigate the N_2 ad-desorption isotherms using liquid nitrogen at 77 K. Moreover, The curves of pore-size distribution of materials was obtained by the traditional Barrett-Joyner-Halenda (BJH) method.

The amount of acid and the type of acid are calculated using the following formula:

$$C_{\text{py-B}} = \frac{1.88 I_{\text{A(B)}} R^2}{W};\ \left(1.88 = \frac{\pi}{\varepsilon_{\text{B}}}, \varepsilon_{\text{B}} = 1.67 \pm 0.1 \text{cm}/\mu\text{mol}\right)$$

$$C_{\text{py-L}} = \frac{1.42 I_{\text{A(L)}} R^2}{W};\ \left(1.42 = \frac{\pi}{\varepsilon_{\text{L}}}, \varepsilon_{\text{L}} = 2.22 \pm 0.1 \text{cm}/\mu\text{mol}\right)$$

where $C_{\text{py-B}}$ and $C_{\text{py-L}}$ represent the concentration of Brønsted and Lewis acids, respectively. $I_{\text{A(B)}}$ and $I_{\text{A(L)}}$ represent the integrated absorbance of Brønsted and Lewis acids, respectively. R is the radius of the wafer (cm). W is weight of wafers (mg).

2.5. ACE testing

The catalytic properties of FCC catalysts were evaluated at Lanzhou Petrochemical Research Center, using the ACE unit Model R+MM from Kayser Technology. The fluidization of the reactor was achieved by a stream of nitrogen. 9 g catalyst was fluidized and stabilized at catalyst/oil ratio 5 and the reaction temperature 530 °C.

2.6. Properties of feeding heavy oil

The feeding heavy oil was characterized with viscosity 10.38–14.35 mm^2/s, residual carbon 3.4–4.2 wt%, and density 900 kg/m^3.

3. Results and discussion

3.1. Hydrothermal stability

~25 tons of MAs were manufactured at a commercial zeolite manufacturing corporation by using the existing production equipments. This is the first time that MAs are manufactured at an industrial scale. Characterization results (Fig. 1 and Fig. 2) showed that the industrial product had similar physicochemical properties with those obtained at the laboratory. With a BET surface area of 769 $m^2\ g^{-1}$, the industrial product has a narrow mesopores centered around 3.5–4.5 nm (Fig. 3). After the hydrothermal deactivation at 800 °C for 10 h under 100% water vapor, the total surface area decreased from 769 $m^2\ g^{-1}$ to 154 $m^2\ g^{-1}$, the total pore volume decreased from 0.77 cm^3/g to 0.32 cm^3/g, while the mesopore volume dropped from 0.57 cm^3/g to 0.25 cm^3/g (Table 1). Interestingly, the diameter and the size distribution of mesopores became wider (Fig. 3). All these results demonstrated the excellent hydrothermal stability of industrial products. TEM images (Fig. 4)

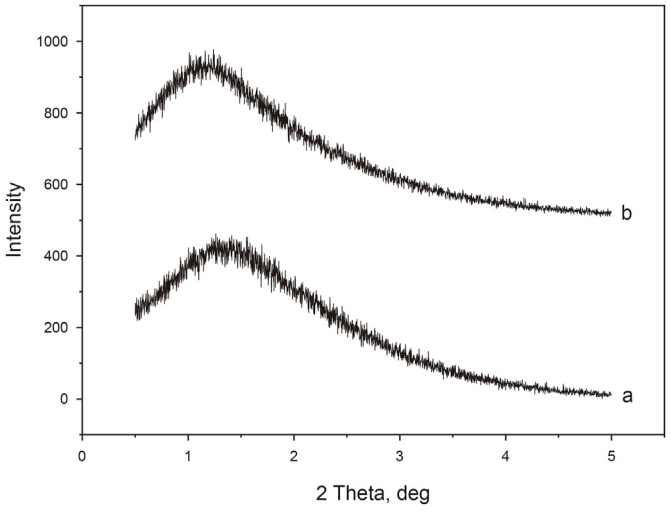

Fig. 1. XRD patterns for the obtained materials: (a) IS, and (b) HIS.

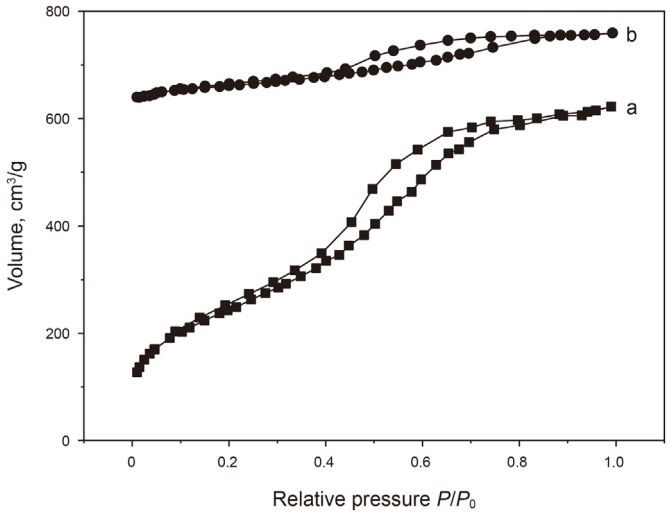

Fig. 2. N_2 ad-desorption isotherms of the obtained products: (a) IS, and (b) HIS.

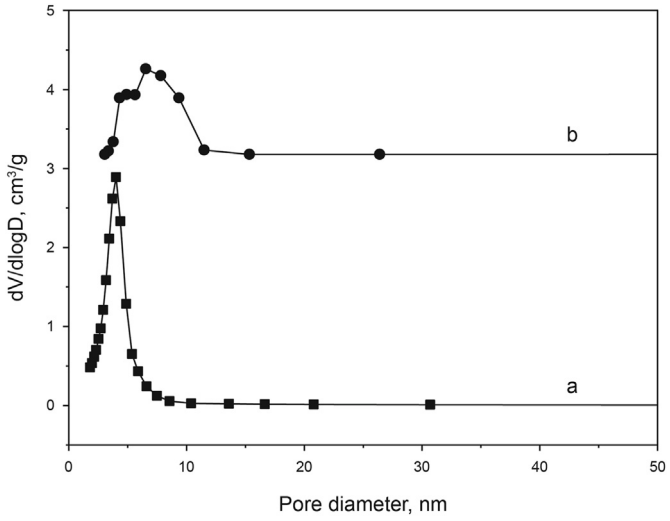

Fig. 3. Curves of pore size distribution of the obtained products: (a) IS, and (b) HIS.

showed that IS after the severe hydrothermal ageing still exhibited mesoporous structure which is typically wormlike, suggesting the high hydrothermal stability of IS.

3.2. Acidity characteristics

The MAs was milled and then mixed with kaolin, rare earth salts, pseudo-boehmite, and alumina sol. The mixtures are spray-dried into 429 tons of FCC catalysts microspheres with the diameter of 75 μm. The final catalyst was named "LPC-65". The incumbent catalyst applied in the industrial FCC unit LDO-70 was used to compare with LPC-65.

To study the acidity characteristics of LDO-70 and LPC-65, Brønsted acid sites (BAS) and Lewis acid sites (LAS) were calculated from Py-FTIR spectra in the temperature range of 473–623 K, and the corresponding results were depicted in Fig. 5, Fig. 6 and Table 2. From Table 2, we could see that both the total acid sites and the BAS of LPC-65 are much higher than those of LDO-70. In this sense, it could be reasonably deduced that the conversion of heavy oil would increase greatly.

3.3. Catalytic cracking properties of catalysts in ACE

The final catalyst LPC-65 exhibited a total surface area of 258 $m^2\ g^{-1}$, including micropores area of 173 $m^2\ g^{-1}$ and mesopores area of 85 $m^2\ g^{-1}$ (Table 3). As for comparison, the incumbent industrial catalyst LDO-70 has a total surface area of 239 $m^2\ g^{-1}$, including micropores area of 169 $m^2\ g^{-1}$ and mesoporosity surface area of 70 $m^2\ g^{-1}$.

LPC-65 and LDO-70 were hydrothermally deactivated at 800 °C for 4 h under 100% water vapor to simulate the catalytic properties of equilibrium catalysts. The mesoporous surface area of steamed LPC-65 is 195 $m^2\ g^{-1}$, in which the mesoporous surface area is 64 $m^2\ g^{-1}$, much higher than that of the reference catalyst (49 $m^2\ g^{-1}$), indicating that the remaining ratio of mesoporosity is high even after severe hydrothermal treatment. ACE test of the two deactivated catalysts using the same heavy oil feed suggested the clear advantage of LPC-65 in selectivity, mainly in increased conversion of 3.36%, reduced heavy oil yield of 1.39% and increased total liquid yield of 0.67% (Table 4). The lower coke factor of LPC-65 compared with that of LDO-70 exhibited much enhanced selectivity, which was the most important factor for FCC catalysts. These interesting results could be reasonably ascribed to the presence of enhanced hydrothermally stable mesoporosity.

It is well known that vanadium and nickel will cause damage to zeolites in FCC conditions (Trujillo et al., 1997; Xu et al., 2002; Hagiwara et al., 2003; Cerqueira et al., 2008). The ACE test of the contaminated LPC-65 and LDO-70 (deactivated with 3000 ppm Ni and 5000 ppm V) suggested the clear advantage of contaminated LPC-65 in selectivity, mainly in increased conversion of 4.48%, reduced heavy oil yield of 2.82% and increased total liquid yield of 2.14% (Table 5). These results demonstrated that the obtained MAs could withstand the severe conditions in industrial FCC units. To the best of our knowledge, this is the first time that a mesoporous aluminosilicate demonstrated excellent hydrothermal stability in FCC units. Moreover, it is the first time that a mesoporous aluminosilicate is employed in FCC catalysts with good activity and selectivity.

3.4. Catalytic cracking properties of catalysts in industrial FCC unit

LPC-65 was added to 1.2-million tons equipment at the same addition rate with that of the incumbent catalyst. As a result of this, a constant catalyst inventory of 429 tons was maintained in the industrial unit. The change-over from the incumbent catalyst to LPC-65 resulted in an 83.37% inventory ratio at the end of 68 days trial. Equilibrium catalyst samples in different inventory ratios were collected and characterized periodically. Interestingly, the surface area of trial equilibrium catalysts (30% inventory ratio) increased from 110 $m^2\ g^{-1}$ to 120 $m^2\ g^{-1}$, consistent with the higher

Table 1
XRD and BET characterization results of IS, and HIS.

Sample	2-Theta	Area	S_{BET}, $m^2 \cdot g^{-1}$	S_{MES}, $m^2 \cdot g^{-1}$	S_{MIC}, $m^2 \cdot g^{-1}$	V_{Total}, $cm^3 \cdot g^{-1}$	V_{MES}, $cm^3 \cdot g^{-1}$	V_{MIC}, $cm^3 \cdot g^{-1}$	D_{avg}, nm
IS	1.16	913	769	713	56	0.77	0.57	0.20	3.2
HIS	1.41	255	154	125	29	0.32	0.25	0.07	6.5

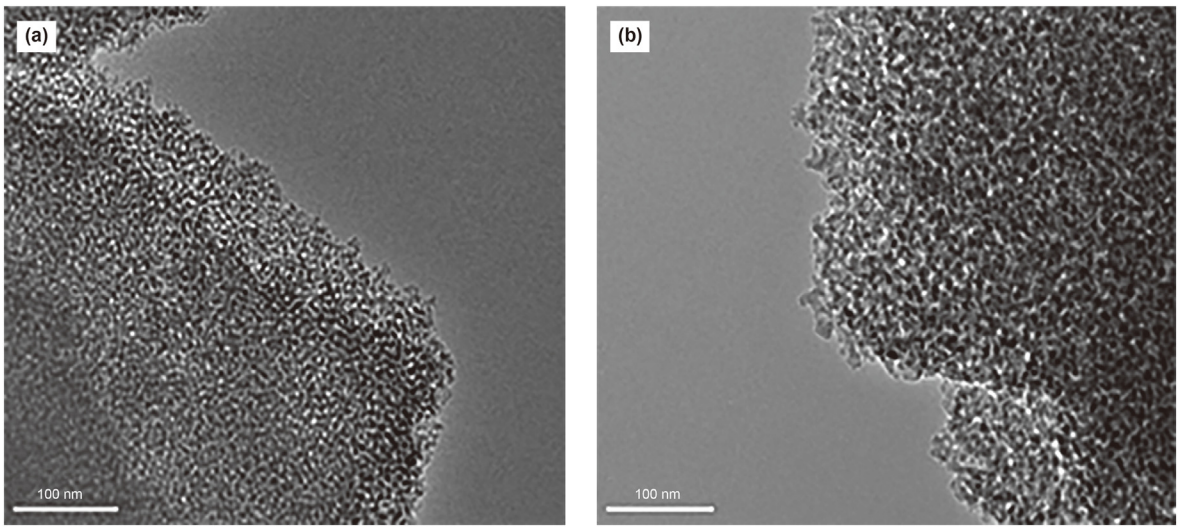

Fig. 4. TEM images of samples: (**a**) IS, and (**b**) HIS.

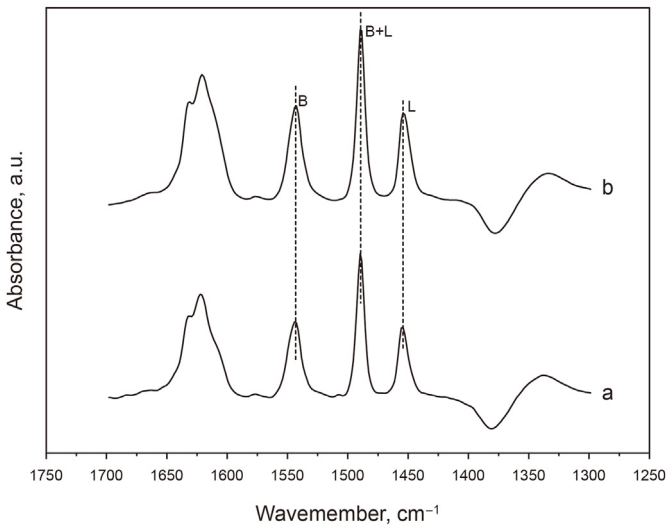

Fig. 5. Py-IR spectra of (a) LDO-70, and (b) LPC-65 at 200 °C.

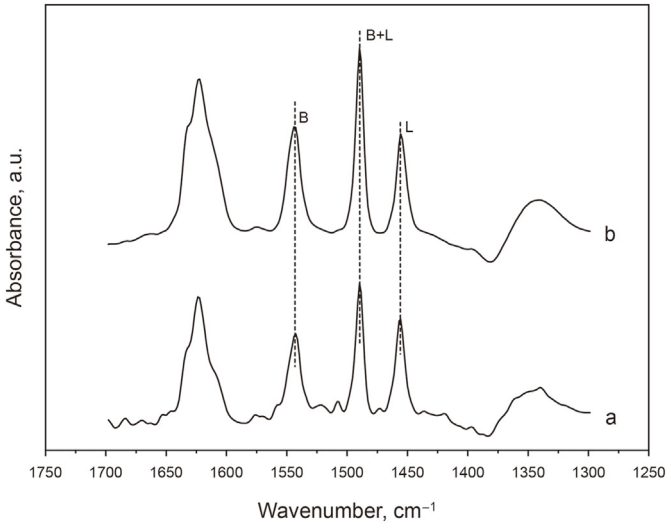

Fig. 6. Py-IR spectra of (a) LDO-70, and (b) LPC-65 at 350 °C.

surface area of fresh LPC-65. Surprisingly, a significant increase in the mesoporous surface area of trial equilibrium catalysts (30% inventory ratio) from 33 $m^2\ g^{-1}$ to 40 $m^2\ g^{-1}$ (22% increase), indicating the high hydrothermal stability of the mesoporosity in this industrial unit.

Table 6 summarized the industrial results of equilibrium catalysts of the incumbent and LPC-65. Compared with LDO-70, the equilibrium catalyst that contain 80% LPC-65 yields significantly lower heavy oil (0.23%) and higher total liquids (0.53%). These results are very close to those obtained from laboratory ACE testing. Generally, the activity of equilibrium catalyst could be considered as the average activity of all the catalyst in FCC unit, which included fresh catalyst and deactivated catalyst. Therefore, it could be suggested that LPC-65 was an ideal FCC catalyst.

Mechanical resistance is another important quality of FCC catalyst, because it reduces the flow of catalyst that must be purged. Interestingly, the abrasion index of LPC-65 is 1.6, much lower than the prerequisite value 3.0. These results indicated that LPC-65 developed in this paper had comprehensive advantages compared with the commercial catalysts.

Table 2
Acid amount and acid type of LDO-70, and LPC-65.

Sample	Weak acid sites, μmol/g			Strong acid sites, μmol/g			Total acid sites, μmol/g
	B	L	B + L	B	L	B + L	
LDO-70	84	41	125	50	35	85	210
LPC-65	139	77	216	72	39	111	327

4. Conclusions

For the first time, mesoporous aluminosilicates with excellent hydrothermal stability were manufactured at the commercial scale by a unique process. FCC catalysts obtained from the MAs exhibited high stability in an industrial FCC unit. The catalyst showed improved product selectivity compared with the incumbent catalyst, at a high inventory ratio of 80%. Gasoline oil yield with 80% LPC-65 equalized catalyst enhanced by 1.22% and the total liquid yield enhanced by 0.53%. The results of synthesis and application

Table 3
Physicochemical properties of catalysts.

Sample	Na_2O, wt%	RE_2O_2, wt%	S_{BET}, m^2/g	S_{MIC}, m^2/g	S_{MES}, m^2/g	V_{Total}, cm^3/g
LPC-65	0.10	2.64	258	173	85	0.42
LDO-70	0.11	2.81	239	169	70	0.38
Steamed LPC-65[a]			195	131	64	0.30
Steamed LDO-70[a]			168	119	49	0.26
Incumbent equilibrium catalyst			110	77	33	0.15
Catalyst change-out, 30%			120	80	40	0.17
Catalyst change-out, 50%			121	79	42	0.16
Catalyst change-out, 80%			126	79	47	0.19

[a] LPC-65 and LDO-70 were hydrothermally deactivated at 800 °C for 4 h under 100% water vapor.

Table 4
ACE testing results of catalysts.

	Steamed LDO-70[a]	Steamed LPC-65[a]
Dry gas, wt%	2.04	2.24
LPG, wt%	19.60	20.75
Gasoline, wt%	53.11	54.49
Diesel, wt%	12.60	10.75
Heavy oil, wt%	5.81	4.42
Coke, wt%	6.83	7.36
Conversion, wt%	81.58	84.94
Total liquids, wt%	85.32	85.99
Coke factor[b]	1.54	1.30

[a] LPC-65 and LDO-70 were hydrothermally deactivated at 800 °C for 4 h under 100% water vapor.
[b] Coke factor $= Y_{Coke} \times (100-X)/X$, which Y_{Coke} is coke yield, X is conversion ratio.

Table 5
ACE testing resulting of contaminated LPC-65 and contaminated LPC-70.

	Contaminated LPC-65[a]	Contaminated LDO-70[a]
Dry gas, wt%	3.13	3.14
LPG, wt%	19.72	16.35
Gasoline, wt%	41.28	40.60
Diesel, wt%	15.07	16.99
Heavy oil, wt%	10.68	13.50
Coke, wt%	9.87	9.43
Conversion, wt%	73.99	69.51
Total liquids, wt%	76.07	73.93
Coke factor	3.465	4.136

[a] Contaminated with 3000 ppm Ni and 5000 ppm V, and hydrothermally aged in 800 °C, 100% water vapor for 4 h.

Table 6
Catalytic performance of LDO-70 and catalyst with change-out of LPC-65.

Catalyst change-out	LPC-65	LPC-65	LPC-65	LPC-65
	0 Equilibrium catalyst LDO-70	30%	50%	80%
Dry gas, wt%	3.75%	3.45%	3.38	3.52%
LPG, wt%	17.64%	18.08%	18.32	18.07%
Gasoline, wt%	48.46%	49.26%	49.08	49.68%
Diesel, wt%	17.31%	16.23%	16.07	16.19%
Heavy oil, wt%	3.25%	3.15%	3.25	3.02%
Coke, wt%	9.59%	9.83%	9.9	9.52%
Total liquids, wt%	83.41%	83.57%	83.47	83.94%

represent the most advanced development of MAs in heavy oil FCC to date, which bring a ray of hope for the industry-scale application of MAs in heavy oil FCC.

Acknowledgments

The authors acknowledge PetroChina Co. Ltd. for financial support through the research programs (Grant Nos. DQZX-KY-21-008, KYWX-21-023, and KYWX-21-022).

References

Cao, L., Zhao, X., Jin, J., et al., 2014. Crystal-seeds-based strategy for the synthesis of hydrothermally stable mesoporous aluminosilicates with a largely decreased H_2O amount. Ind. Eng. Chem. Res. 53 (44), 17286–17293. https://doi.org/10.1021/ie502934q.
Cerqueira, H.S., Caeiro, G., Costa, L., et al., 2008. Deactivation of FCC catalysts. J. Mol. Catal. Chem. 292 (1), 1–13. https://doi.org/10.1016/j.molcata.2008.06.014.
Chen, H., Zhen, F., Liu, H., et al., 2021. Hydrophobic polypropylene glycol integration into the micelles: a general approach for high utilization efficiency of organic template. Ind. Eng. Chem. Res. 60, 9482–9488. https://doi.org/10.1021/acs.iecr.1c01500.
Corma, A., Corresa, E., Mathieu, Y., et al., 2017. Crude oil to chemicals: light olefins from crude oil. Catal. Sci. Technol. 7 (1), 12–46. https://doi.org/10.1039/C6CY01886F.
Deng, Y., Zhou, J., Li, G., et al., 2022. Synthesis of well-ordered mesoporous aluminosilicates with high aluminum contents: the challenge and the promise. Inorg. Chem. 61, 11820–11829. https://doi.org/10.1021/acs.inorgchem.2c01571.
Fu, J., Kim, S., Rodgers, R.P., et al., 2006. Nonpolar compositional analysis of vacuum gas oil distillation fractions by electron ionization fourier transform ion cyclotron resonance mass spectrometry. Energy Fuel. 20 (2), 661–667. https://doi.org/10.1021/ef0503515.
Hagiwara, K., Ebihara, T., Urasato, N., et al., 2003. Effect of vanadium on USY zeolite destruction in the presence of sodium ions and steam-studies by solid-state NMR. Appl. Catal. A-Gen. 249 (2), 213–228. https://doi.org/10.1016/S0926-860X(03)00289-8.
Jin, J., Cao, L., Hu, Q., et al., 2014. An efficient synthesis of hydrothermally stable mesoporous aluminosilicates with significant decreased organic templates by a seed-assisted approach. J. Mater. Chem. A. 2 (21), 7853–7861. https://doi.org/10.1039/C4TA00075G.
Ji, D., Wang, B., Yue, T., et al., 2018. Zeolite Beta precursors as building units toward enhancing the microporosity fraction of mesoporous aluminosilicates. Ind. Eng. Chem. Res. 57 (31), 10234–10240. https://doi.org/10.1021/acs.iecr.8b01821.
Jia, X., Khan, W., Wu, Z., et al., 2019. Modern synthesis strategies for hierarchical zeolites: bottom-up versus top-down strategies. Adv. Powder Technol. 30 (3), 467–484. https://doi.org/10.1016/j.apt.2018.12.014.
Kerstens, D., Smeyers, B., Van Waeyenberg, J., et al., 2020. State of the art and perspectives of hierarchical zeolites: practical overview of synthesis methods and use in catalysis. Adv. Mater. 32 (44), 2004690. https://doi.org/10.1002/adma.202004690.
Liu, H., Wang, L., Feng, W., et al., 2013a. Hydrothermally stable bimodal aluminosilicates with enhanced acidity by combination of zeolite Y precursors assembly and the pH-adjusting method. Ind. Eng. Chem. Res. 52 (10), 3618–3627. https://doi.org/10.1021/ie302604m.
Liu, H., Wang, J., Feng, W., et al., 2013b. Synthesis of La-substituted aluminosilicates with hierarchical pores by pH-adjusting method. J. Alloys Compd. 557, 223–227. https://doi.org/10.1016/j.jallcom.2012.12.151.
Liu, H., Guo, K., Li, X., et al., 2014a. Understanding and direct strategy to synthesize hydrothermally stable micro-mesoporous aluminosilicates with largely enhanced acidity. Microporous Mesoporous Mater. 188, 108–117. https://doi.org/10.1016/j.micromeso.2013.11.039.
Liu, H., Zhao, X., Chen, P., et al., 2014b. Hydrothermally stable mesoporous aluminosilicates with moderate acidity via degradation-assembly process and improved catalytic properties. J. Porous Mater. 21, 379–386. https://doi.org/10.1007/s10934-014-9783-x.
Liu, H., Wang, K., Shi, Y., et al., 2014c. Hydrothermally stable macro-meso-microporous materials: synthesis and application in heavy oil cracking. RSC Adv. 4, 29694–29697. https://doi.org/10.1039/C4RA03752A.
Liu, H., Zhang, Y., Lv, L., et al., 2021. Obtaining of mesoporous aluminosilicates with high hydrothermal stability by composite organic templates: utility and mechanism. Langmuir 37, 9137–9143. https://doi.org/10.1021/acs.langmuir.1c01151.
Li, Y., Xi, Y., Gao, X., et al., 2022. Preparation of mesoporous aluminosilicates with decreased dosage of organic template and water: insights into the HLB effect of the contemplate. Ind. Eng. Chem. Res. 61, 15796–15802. https://doi.org/10.1021/acs.iecr.2c02609.
Mi, X., Liu, H., Wang, B., et al., 2017a. Urea as efficient additive toward decreasing

water amount in synthesis of hydrothermally stable mesoporous aluminosilicates. Ind. Eng. Chem. Res. 56 (33), 9401–9407. https://doi.org/10.1021/acs.iecr.7b02362.

Mi, X., Yuan, J., Han, Y., et al., 2017b. Introduction of anionic surfactants to copolymer micelles: a key to improving utilization efficiency of P123 in synthesis of mesoporous aluminosilicates. Ind. Eng. Chem. Res. 56 (25), 7224–7228. https://doi.org/10.1021/acs.iecr.7b01142.

Mi, X., Wang, J., Li, J., et al., 2018a. A facile strategy to synthesize hydrothermally stable mesoporous aluminosilicates with significantly decreased organic templates and H_2O. Colloid. Surface. 558, 179–185. https://doi.org/10.1016/j.colsurfa.2018.08.078.

Mi, X., Liu, H., Wang, B., et al., 2018b. Synthesis of hydrothermally stable mesoporous aluminosilicates by using urea as additive. Mater. Chem. Phys. 208, 220–225. https://doi.org/10.1016/j.matchemphys.2018.01.026.

Puente, G.D.L., Devard, A., Sedran, U., 2007. Conversion of residual feedstocks in FCC. Evaluation of feedstock reactivity and product distributions in the laboratory. Energy Fuel. 21 (6), 3090–3094. https://doi.org/10.1021/ef700313u.

Palos, R., Gutierrez, A., Vela, F.J., et al., 2021. Waste refinery: the valorization of waste plastics and end-of-life tires in refinery units. A review. Energ. Fuel. 35 (5), 3529–3557. https://doi.org/10.1021/acs.energyfuels.0c03918.

Saxena, S.K., Viswanadham, N., Sharma, T., 2014. Breakthrough mesopore creation in BEA and its enhanced catalytic performance in solvent-free liquid phase tert-butylation of phenol. J. Mater. Chem. A. 2 (8), 2487–2490. https://doi.org/10.1039/C3TA14784C.

Trujillo, C.A., Uribe, U.N., Knops-Gerrits, P.P., et al., 1997. The mechanism of zeolite Y destruction by steam in the presence of Vanadium. J. Catal. 168 (1), 1–15. https://doi.org/10.1006/jcat.1997.1550.

Talmadge, M.S., Baldwin, R.M., Biddy, M.J., et al., 2014. A perspective on oxygenated species in the refinery integration of pyrolysis oil. Green Chem. 16 (2), 407–453. https://doi.org/10.1039/C3GC41951G.

Verboekend, D., Keller, T., Mitchell, S., et al., 2013. Zeolites: hierarchical FAU-and LTA-type zeolites by post-synthetic design: a new generation of highly efficient base catalysts. Adv. Funct. Mater. 23, 1923–1934. https://doi.org/10.1002/adfm.201370073.

Valle, B., Remiro, A., García-Gómez, N., et al., 2019. Recent research progress on bio-oil conversion into bio-fuels and raw chemicals: a review. J. Chem. Technol. Biot. 94 (3), 670–689. https://doi.org/10.1002/jctb.5758.

Xu, M., Liu, X., Madon, R.J., 2002. Pathways for Y zeolite destruction: the role of Sodium and Vanadium. J. Catal. 207 (2), 237–246. https://doi.org/10.1006/jcat.2002.3517.